Plasmon nanoparticle array waveguides for single photon and single plasmon sources

A. Femius Koenderink*

Center for Nanophotonics, FOM Institute for Atomic and Molecular Physics (AMOLF), Science Park 104, 1098 XG Amsterdam, The Netherlands

E-mail: f.koenderink@amolf.nl

Abstract

This Letter discusses how linear coupled plasmon particle arrays inspired by radio frequency Yagi-Uda antennas can be used to construct both efficient uni-directional single photon sources and efficient directional single plasmon sources. Calculations using an exact multipole expansion method are presented of the spontaneous emission directivity, efficiency and spontaneous emission decay rates, taking into account material loss in real noble metals. An analysis of the emission properties in terms of the dispersion relation of infinite arrays reveals how one can use guided mode dispersion to achieve desirable figures of merit. Key ingredient is to couple the source to array eigenmodes that are just beyond the light line, but still wave vector matched to propagating modes to within the momentum uncertainty set by the inverse antenna length. Finally, this Letter shows that the emission decay rates can be controlled independently of the directionality and without penalty in quantum efficiency.

Efficient coupling of single quantum systems to single photons is of core interest for all optics-based quantum information processing schemes.[1–3] For instance, single photon sources for secure quantum communication can be reliably achieved by using a single two-level system that emits

into a single optical mode.[4] Similarly, efficient coupling of a single emitter to a single mode is required for exchanging quantum states of localized qubits with quantum states of photons, or for proposed 'single photon transistors', where a single quantum system can be switched by absorbing a single photon with unit probability.[5,6] The conventional strategy to reach such single-photon devices is to couple a two-level system to a high quality factor (Q) microcavity with a low mode volume (V). Purcell enhancement ensures preferential emission into a single confined mode[4,7,8] at high rate. However, the confined nature of microcavity modes makes it a challenge to collect the light efficiently into a unique propagating channel, and the required high Q's imply very narrow operation band widths.

Recently, plasmon structures have gained attention as broadband structures to control single emitters.[9–17] On the one hand Akimov, Chang, and Falk *et al*. have proposed and demonstrated single plasmon sources and detectors based on Purcell-enhanced decay of quantum dots into Ag nanowire plasmon modes.[5,18–20] On the other hand, several groups have independently proposed to create photon sources by using plasmon scatterers to mimick microwave antennas.[13,14,16] Design requirements for microwave antennas are similar as for single photon sources: a high emission power per input current is desired, as is high directionality for efficient sending of signals. However, the archetypical uni-directional microwave antenna is not based on high Q, low V resonances, but is based on coherent multiple scattering in systems that consist of resonant scatterers[21] arranged in arrays of subwavelength pitch. The geometrical configuration of the scatterers determines the spatial coherence of the emitted signal that translates into a high directivity.

In this Letter the coupling of emitters to plasmon nanosphere chains as sketched in Figure 1(A) is explained based on exact electrodynamical calculations. The analysis demonstrates the effectiveness of such nanoparticle chains as antennas for directional single photon sources, and quantitatively explains the directionality and quantum efficiency in terms of the mode structure of the arrays.[22] Moreover, results show that the same plasmon chains can also be used to create single plasmon sources, when operated in a different frequency band. This is a highly surprising result, since the figures of merit of single plasmon sources and plasmon-assisted single photon sources

are completely opposite. The objective of a single photon source is that all emission events lead to photons in the far field, rather than remaining confined, as is required for a plasmon source. We uncover a general design route based on wave vector matching for creating single photon sources and single plasmon sources within a single system. Simple nanosphere directional antennas do not strongly enhance transition rates. A simple modification is proposed that provides large increases in radiative decay rate, without a penalty in quantum efficiency or directionality.

The results reported in this Letter are calculated using an exact electrodynamic multiple scattering multipole expansion method called 'MESME' developed and made available by F. J. García de Abajo in order to rigorously solve Maxwell's equations[23,24] for finite clusters of scatterers. Earlier work on Yagi-Uda plasmon antennas either used point dipole models[13,14] or brute force Finite Difference Time Domain simulations (FDTD).[16] In contrast, MESME is an anlytical method that includes all multipole expansion terms, meaning that emission rate modifications and local field enhancements that are inaccessible to point dipole methods are calculated exactly. At the same time, this quasi-analytical method is sufficiently fast to explore many geometries, as opposed to FDTD. In brief, MESME expresses the fields scattered by each plasmon particle as a multipole expansion. The multipole excitations on each particle are driven both by the incident field and by the fields associated with all other particles, giving rise to a set of self-consistent equations for the multipole expansion coefficients that is solved recursively.[23,24] To obtain results that are converged to within 0.1 percent, $l = 30$ multipoles per particle, and up to 25 scattering orders (*i.e.* recursions) are used. The method was succesfully benchmarked against reported literature for the response of clusters of dielectric and plasmonic spheres to far-field illumination.[25–27]

In order to deal with the interaction of antennas with fluorophores, I extended MESME to model monochromatically oscillating localized dipole currents, rather than plane wave incident fields. To retrieve spontaneous emission rates additional calculations are required, beyond the near-field spatial distribution and far-field angular distribution of radiation. Spontaneous emission rates are determined from the integrated far-field radiated power $P_{\mathrm{rad}} = \int_{2\pi\ \mathrm{sr}} \frac{dP}{d\Omega} d\Omega$ at fixed dipole current, and from the total work per unit time $P_{\mathrm{total}} = \mathrm{Im}(\mathbf{j}^* \cdot \mathbf{E}(\mathbf{r}_{\mathrm{source}}))$ that the electric field

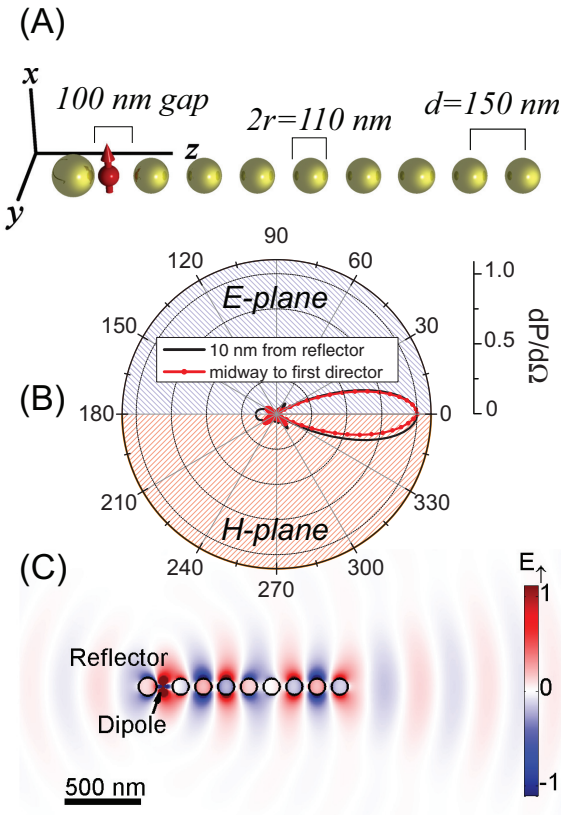

Figure 1: (Color) (A) Sketch of a plasmon nanosphere Yagi-Uda antenna consisting of one oriented emitter (red), one reflector particle, and an equidistant array of eight director particles. The antenna is embedded in glass, and consists of Ag nanospheres(tabulated optical constants[28]). (B) Emission pattern for emission at $\lambda = 650$ nm, taking eight directors with a radius of $r = 55$ nm, and with a pitch of $d = 150$ nm. The emission pattern represents the power emitted per steradian ($dP/d\Omega$) normalized to the forward emitted power. The emission pattern is almost identical for a molecule placed midway in the 100 nm gap between reflector and 1st director (red curve), and for a molecule at a distance of 10 nm from the reflector (black curve). The upper (lower) half of the diagram (shaded blue (red)) summarizes emission in the xz (yz) plane, showing that the angular width of the emission cone (3dB half width, i.e. angle for which $dP/d\Omega = 0.5$) is around 15° (see Figure 3(B)).(C) Snapshot in the xz plane of the x-component of the electric field induced by the radiating dipole.

$E(\mathbf{r})e^{i\omega t}$ radiated by the imposed dipole current $\mathbf{j}e^{i\omega t}\delta(\mathbf{r}-\mathbf{r}_{\text{source}})$ located at $\mathbf{r}_{\text{source}}$ does on the dipole current itself.[29–32] By normalizing the two powers P_{rad} and P_{total} to the power P_0 radiated by the same current in vacuum, one obtains the radiative rate enhancement $\Gamma_{\text{rad}} = P_{\text{rad}}/P_0$ and the total decay rate enhancement $\Gamma_{\text{total}} = P_{\text{total}}/P_0$ for a fluorophore, relative to its rate in vacuum. The ratio of the two rates yields the quantum efficiency $\eta = \Gamma_{\text{rad}}/\Gamma_{\text{total}}$ for emission in presence of the metal. This quantum efficiency only accounts for quenching in the metal and assumes unit efficiency for the fluorophore in absence of the antenna. The method is easily generalized to deal with fluorophores that do not have unit quantum efficiency.[32] This calculation scheme was verified against textbook calculations for fluorophores near single metal spheres.[32,33]

Figure 1(a) shows a sketch of a fluorophore coupled to a Yagi-Uda antenna array consisting of silver nanospheres arranged in a line embedded in glass. In this work, a refractive index $n = 1.5$ for glass and tabulated complex optical constants of silver and gold[28] are used. The dipole is located between a single 'reflector' particle (leftmost) and an array of 'director' particles, and is assumed to be aligned perpendicularly to the antenna axis. The reflector particle prevents emission into the halfspace to the left of the array, and in radio-frequency practice[21] is chosen to have a red-shifted response compared to the director particles. To this end, its radius 60 nm is chosen 10% bigger than that of the other particles. This design is similar to the design based on silver-coated SiO_2 particles proposed by Li et al.,[13] in which core-shell radii were tuned to modify complex polarizabilities. However, solid particles can be much more simply fabricated, for instance by electron beam lithography,[34,35] while still allowing sufficient resonance tuning through size. Figure 1(B) shows polar plots of the far-field intensity distribution ($dP/d\Omega$ emitted power per steradian) radiated by a dipole source oscillating at a frequency corresponding to vacuum wavelength 650 nm, embedded in the array at a distance 50 nm from the reflector particle surface, *i.e.*, midway between reflector and first director. Contrary to the donut-shaped emission pattern of a free dipole, the emission is strongly directional when coupled to the antenna, with a 3dB half width of about 15 degrees viewed in any cross section through the array axis. This directionality confirms earlier predictions,[13,16] although the larger antenna length in calculations presented here results in a stronger directionality. The

beaming implies a 20 times brightness improvement over a free dipole, and 90% of the emission is in a forward cone that can be completely collected with low numerical aperture far-field optics (NA$\sim 0.3-0.5$). The directionality is very robust against movement of the emitter between reflector and director particles (directionality also shown for dipole-reflector distance of 10 nm in Figure 1(b)). It is remarkable that such large and robust directionality is obtained with a structure just $\lambda/5$ wide, and just 2λ long, compared to the wavelength in vacuum (3λ taking the wavelength in glass).

To provide microscopic insight into the predicted beaming, Figure 1(C) allows to examine the near-field in the antenna excited by the dipole. Figure 1(C) shows a snapshot of the electric field component along the emission dipole. The dipole not only sets up a strong electric field in the particle in its immediate vicinity, but also induces strong transverse dipolar excitations in all other plasmon particles. The amplitude of excitation hardly decays over the length of the array, meaning that the dipole strongly excites plasmons even at the array end (2λ away from the source). The temporal evolution of this field (not shown) indicates that the excitation corresponds to a leaky plasmon wave travelling from the leftmost director particle along the array to the right. Comparison of the phase of this wave with the phase fronts of light emerging from the antenna shows approximate matching between the travelling plasmon wave and free photons propagating in the glass along the array axis. The spherical wave emanating from the antenna clearly has maximum amplitude in a narrow forward cone, consistent with the far-field directionality in Figure 1(B).

To ascertain whether excitation of collective guided plasmon waves, as suggested by the near-field plot, indeed explains the beaming behavior, one needs to understand the chain eigenmodes. The dispersion relation for plasmon chains was recently derived and experimentally validated in Refs. 22,35. Two types of eigenmodes exist, namely transverse modes (dipole moments perpendicular to the chain), and longitudinal modes (dipole moments along the chain). Fluorophores with transition dipoles transverse to the chain as in Figure 1 only excite transverse modes. The real part of this transverse dispersion relation, which is calculated on the basis of a point dipole model, is shown in Figure 2. About halfway the Brillouin zone, the transverse dispersion relation splits

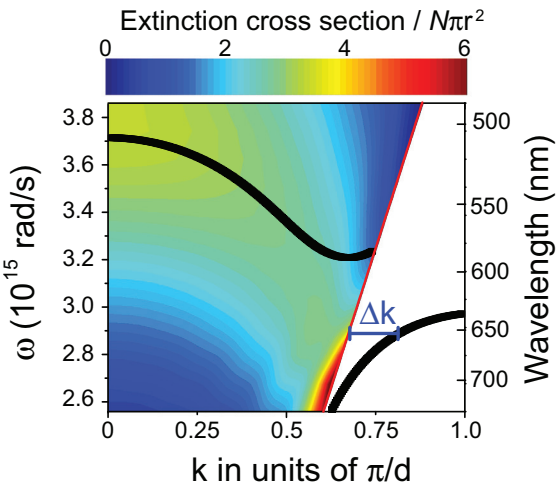

Figure 2: (Color). Black curves: upper and lower dispersion relation for transverse plasmons on an infinite array of director particles (pitch $d = 150$ nm, radius 55 nm). The branches are split by the dispersion of free photons (red line). The background coloring displays the extinction cross section of a finite array of length $L = 10d$ (*i.e.*, 10 particles) of the array as a function of the parallel wave vector of plane wave excitation, and as function of wavelength. Close to the light line, the cross section peaks near the guided mode dispersion branch. Wave vector conservation is only defined to within $\Delta k = \pi/L$ (blue bar).

into two branches, separated by the dispersion relation of free photons propagating in glass ('light line'). The anti-crossing is due to coupling of the localized plasmons to free photon modes.[22] The branch below the light line corresponds to guided modes that only suffer loss from Ohmic damping, while the upper branch corresponds to highly leaky modes with very strong damping due to radiation into the far field.

In order to correlate the infinite chain dispersion to the coupling of finite arrays to far field radiation, I consider the reverse of directional emission, *i.e.*, the response of finite chains to incident plane waves. To this end, the extinction cross section is plotted in Figure 2 versus frequency and incidence angle θ ($\theta = 90^\circ$ is defined as along the array axis), for polarization transverse to the axis of a 10-particle array. Figure 2 shows the cross section as a color scale, plotted as a function of the wave vector component $k_{||} = 2\pi n_{\mathrm{glass}} \sin\theta/\lambda$ parallel to the array. For long arrays, one expects that the extinction peak coincides with the dispersion relation, due to resonant excitation of chain eigenmodes. For light incident normal to the array up to angles of $\approx 70^\circ$, the peak extinction indeed traces the upper branch of the dispersion relation. However, for very large angles (incidence along

the array axis) there is strong scattering in a frequency range that is remarkably red-shifted from the upper dispersion branch. This frequency range matches the guided mode dispersion that is below the light line. At first sight this result is surprising since momentum conservation should forbid light from coupling to the lower dispersion branch. However, for finite arrays (length L), momentum conservation is only defined up to $\Delta k \approx \pi/L$, implying that resonant scattering is possible even from collective array modes with wave vectors beyond, but within Δk of, the light line. It is exactly in this region that both the receiving mode Yagi-Uda antennas studied by de Waele et al.,[36] and the sending mode Yagi-Uda antennas considered in Figure 1(B,C) operate. The mechanism that emerges for directional emission is hence that the emitter preferentially decays into the guided modes of the plasmon array. Within the uncertainty Δk set by the antenna length, these modes are well matched to free photons propagating along the array, giving rise to efficient and strongly directional outcoupling. However, as the emitter is tuned further towards the blue, *i.e.*, into the range where the guided mode wave vector is more than Δk from the light line, one expects no efficient beaming anymore. Instead of acting as a single photon source, the structure acts as a single plasmon source in the sense that the emission remains trapped as a confined slow plasmon, as in the case of the recently reported nanowire-based single plasmon source.[18] However, as opposed to the nanowire source, this source is a *uni-directional* plasmon source due to the presence of the reflector particle.

To validate the prediction that both single photon source and single plasmon source characteristics are governed by how the emission frequency is tuned relative to the guided mode dispersion, it is imperative to examine the spectral dependence of the emission directionality and spontaneous emission decay rates. Figure 3(a) shows the quantum efficiency of the fluorophere embedded in the antenna in Figure 1(a) (again with the dipole at 60 nm away from the reflector particle, assuming unit efficiency for the bare source). Figure 3(b) shows the total decay rate enhancement. Finally, Figure 3(c) displays the dependence of the directionality of the emitted light as a function of wavelength. The directionality, i.e., the width of the emitted cone, is quantified via the angle $\Delta\theta$ from the array axis at which the intensity is 3dB below the on-axis intensity. These figures reveal

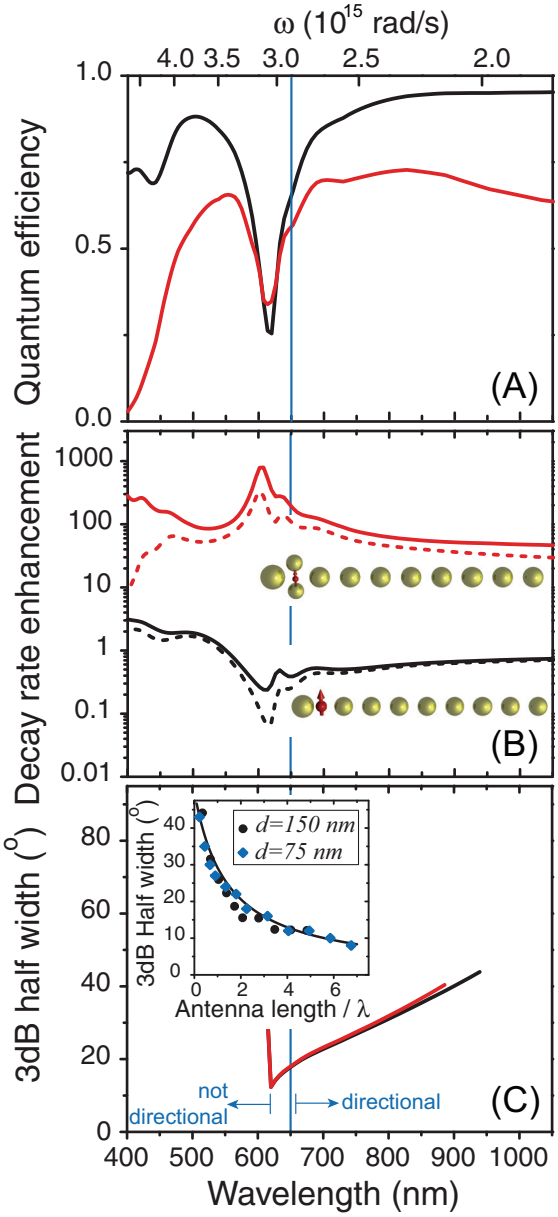

Figure 3: (Color) (A) Quantum efficiency, (B) decay rate enhancement and (C) directionality versus wavelength for the emitter-antenna geometry in Figure 1 (black curves). Red curves show the same results upon replacing the bare emitter with a superemitter configuration with two extra spheres close to the fluorophore (cartoon in (B)). In (B), the solid (dotted) curve represents the total (radiative) decay rate modification. To the red of 650 nm (blue line), the antenna allows efficient and directional emission. To the blue of 650 nm, the efficiency drops due to efficient generation of guided plasmons. The inset in (C) shows the directionality (quantified in (B) and (C) as the angle $\Delta\theta$ at which the radiated power per steradian is at 3dB from the on-axis value), at optimum operation wavelength) versus antenna length L normalized to operation wavelength in the medium, for the antenna with pitch 150 nm considered in Figure 1 and a scaled antenna with pitch 75 nm. The directionality depends inversely on antenna length normalized to emission wavelength with a floor set by the infinite array propagation length L_∞, as indicated by the fitted curve of the form $\sin\Delta\theta = (1/L + 1/L_\infty)$, with $L_{infty} \approx 20\lambda$ set by Ohmic loss.

several remarkable features. First, the total decay rate is not strongly enhanced at any wavelength. In fact, decay is slightly inhibited except in the wavelength range of intraband absorption, where Ag is not a Drude metal. Secondly, the quantum efficiency for emission remains high, except in a narrow band around 625 nm, and thirdly, emission is simultaneously highly efficient ($\eta > 75\%$) and highly directional for wavelengths to the red of ~ 645 nm. For shorter wavelengths, the unidirectional beaming collapses, with emission also in the backward direction and the appearance of more complex multilobed patterns.

Starting at the red end of the spectrum, I correlate these findings with the dispersion relation. The plasmon chain facilitates an efficient directional single photon source from infrared wavelengths down to a cut-off at around 645 nm. The angular cone of emission widens towards the infrared, where the dispersion relation comes closer to the light line, leaving more of the wave vector uncertainty Δk to extend above the light line. Further into the infrared directionality is furthermore reduced because emission is not dominantly into the guided mode when the guided mode is very delocalized.[22] The angular width of emission is narrowest near the cut-off at 645 nm where it collapses very abruptly, coincident with the frequency where the guided mode dispersion relation deviates more than Δk from the light line. In the inset of Figure 3C, I plot the directionality at fixed wavelength ($\lambda = 650$ nm) for antennas with different numbers of directors, i.e., as a function of antenna length L. The result again underlines the importance of antenna length, since the directionality calculated with MESME fits well to a dependence of the form $\sin\Delta\theta \propto \lambda(1/L + 1/L_\infty)$. This form takes into account that the directionality is ultimately limited by Ohmic loss of the array guided mode. Ohmic loss sets a guided mode amplitude loss length around $L_\infty \approx 20\lambda$.[22] The guided mode loss implies that the effective antenna length is always at most L_∞, and hence that the directionality can not be reduced below a few degrees (i.e., $\Delta k = \pi/L_\infty$).

To the blue of 645 nm, down to around 625 nm, the emitted power is mainly funneled into guided plasmons that poorly radiate. Judging from the calculated external quantum efficiency, a 75% fraction of emission is into the transverse guided plasmon wave. This fraction is surprisingly high, given the large distance to any metal surface, and is comparable to the estimated efficiency

for excitation of plasmons in plasmon nanowires.[18] The blue edge of the quantum efficiency drop at 625 nm, *i.e.*, the blue edge of the regime of single plasmon operation, signals the cut-off of the guided mode dispersion. Further to the blue, emission into the upper dispersion branch with extremely short propagation distances shows no clearly defined radiation angles.

In addition to results in Figure 3, calculations for arrays with very different pitches provide further evidence that the single photon/single plasmon source is associated with the lower dispersion branch. Reducing the particle radii and pitch by a factor two (pitch $d = 75$nm) reduces the wavelength for directional emission from 645 nm to approximately $\lambda = 500$ nm (not shown), which is equivalent to $\lambda \sim 4.4d$ (taking the wavelength in glass). Clearly, the operation wavelength is not associated with a fixed geometrical condition on d/λ, as would be the case in grating-assisted effects. The scaling of operation wavelength with pitch is commensurate with the shift of the lower dispersion branch in the dispersion diagram that occurs as r and d change (not shown). This non-trivial shift is associated with the width of the avoided crossing between the branches on either side of the light-line, and is hence tuned via both the pitch and the interparticle coupling strength. The inset in Figure 3(C) shows that the directionality of the $d = 75$ nm antenna maps onto the same inverse antenna length dependence as the directionality of the $d = 150$ nm antenna, provided one expresses the antenna length in units of operation wavelength in the medium. Additional calculations furthermore demonstrate that similar performance in directionality and quantum efficiency is obtained for antennas made from Au particles, although the window of operation is red-shifted (not shown), commensurate with the red-shifted plasmon chain dispersion.

Despite evidence in Figure 1 and Figure 3 for efficient coupling of emission into plasmon chain modes, the total decay rate shows no large enhancement. To understand this, it is important to recall that the transverse dipole orientation required for coupling to transverse array modes implies tangential dipole orientation relative to the adjacent plasmon spheres. From single plasmon sphere analysis,[32] it is known that tangential orientations are disadvantageous for rate enhancements, as the dipole moment induced by the emitter in the adjacent plasmon sphere opposes the dipole moment of the emitter itself. Opposing dipole moments imply destructive far-field interference of the

fields radiated by emitter and particle (which are comparable in size), and hence no rate enhancement. Conversely, radial dipole orientations cause alignment of the induced plasmon dipole with the emitter, and hence enhanced emission rates. This behavior is counterintuitive with respect to the physics of cavities embodied in the Purcell factor: in the plasmon case the rate enhancement *is not* a measure for how strongly the dipole couples to the localized plasmon resonance. Indeed, the magnitude of the induced dipole in the plasmon particle is comparable for all orientations, even though the rates of decay strongly differ.

By sandwiching the dipole radially between two extra plasmon particles (taken in Figure 3 (red curves, upper cartoon in (b)) as 40 nm in radius, with a 20 nm gap for the emitter), emission rate enhancements between 10^2 and 10^3 can be obtained. This modification constitutes a replacement of the original emitter with a 'superemitter', as first realized by Farahani*et al.*[10] in the context of bow-tie antennas. The 'super-emitter' not only enhances rates, but has the added benefit of effectively pinning the emission dipole to be transverse to the array, independently of the actual physical orientation of the fluorophore. This functionality is similar to the use of elongated metal particles to create antenna arrays as suggested by Taminiau et al. in Ref. 16. To within a few percent, no modification of the radiation pattern occurs upon insertion of the super-emitter, and the penalty in quantum efficiency is limited as shown in Figure 3(a). While the directionality of the bare antenna is only maintained for fluorophores that have their transition dipole oriented within a 30° angle of the transverse direction (about 10% of all dipole orientations), the 'super-emitter' antenna causes directional emission at enhanced rate for over 90% of all possible fluorophore orientations, i.e., for all orientations except those within 5° of the array axis. As Figure 3 shows, the 'super-emitter' strategy allows to control the total emission rate without a large penalty in quantum efficiency or a change in directionality. Of course the particular solution proposed here and in Ref. 16 does break the transverse polarization degeneracy that could have been advantageous for quantum information applications. Alternative solutions to maintain degeneracy while enhancing rates can be obtained with more complex out-of-plane super-emitter constructs, or conversely by placing the Yagi-Uda antenna without superemitter in a classical microcavity.

In conclusion, both novel single plasmon sources and plasmon-assisted single photon sources can be designed from finite segments of plasmon particle wave guides. Phase matching of the guided mode with free photons to within the wave vector uncertainty set by the antenna length is sufficient to ensure directional emission. When the emitter is resonant with guided modes that have a larger wave vector mismatch with free photons, no directional emission occurs and emission is into the truly guided polariton mode. It is well known in antenna theory[21] that many directional antennas are so-called 'travelling wave' antennas, in which elements along the antenna length are driven with phase differences matched to free photons. Indeed, this is the essential philosophy of phased array antennas, in which all elements are actively and independently driven with a current of controlled amplitude and phase. In optics, as in Yagi-Uda antennas, one has only one active element, that induces a response in all other elements. This Letter shows that antenna design does not need a full brute force multiple scattering solution to find all induced phases, as is often used.[21] Instead the dispersion relation for infinite array traveling eigenmodes naturally allows the design of traveling wave antennas simply based on matching of wave vector. Hence, the principles proposed here will benefit the design of directional sources also in many other systems, such as (periodically corrugated) plasmon wires,[5,18,20] semiconductor nanowires,[37] as well as metamaterial arrays ranging from visible to microwave frequencies.[38] The near-unit efficiency coupling of emitters to photonic systems that is used to create directional sources does not imply large decay rate enhancements. By adapting the local subwavelength surroundings of the emitter within the larger antenna structure, one can change the decay rate enhancement factor independently of the directionality. Plasmon nano-systems can thus combine Purcell factors that are competitive with those of microcavity single photon sources with large brightness enhancements due to enhanced directionality. Even when taking quenching into account, plasmon antennas can provide a competitive route to broadband single photon sources.

Acknowledgement

I am especially indebted to Javier García de Abajo for providing the MESME source code, and

for stimulating discussions regarding the adaptation of MESME to spontaneous emission problems. I furthermore acknowledge Albert Polman for discussions and Tobias Kampfrath for careful reading of the manuscript. This work is part of the research program of the "Stichting voor Fundamenteel Onderzoek der Materie (FOM)," which is financially supported by the "Nederlandse Organisatie voor Wetenschappelijk Onderzoek (NWO)." Furthermore, I acknowledge a VENI fellowship funded by NWO.

References

(1) Grangier, P.; Abram, I. *Physics World* **2003**, *16(2)*, 31–35.

(2) *The Physics of quantum information: Quantum cryptography, quantum teleportation, quantum computation*; Bouwmeester, D., Ekert, A. K., Zeilinger, A., Eds.; Springer: Berlin, 2000.

(3) Gisin, N.; Ribordy, G. G.; Tittel, W.; Zbinden, H. *Rev. Mod. Phys.* **2002**, *74*, 145–195.

(4) Lounis, B.; Orrit, M. *Rep. Prog. Phys.* **2005**, *68*, 1129.

(5) Chang, D. E.; Sørensen, A. S.; Demler, E. A.; Lukin, M. D. *Nature Physics* **2007**, *3*, 807–812.

(6) Hwang, J.; Pototschnig, M.; Lettow, R.; Zumofen, G.; Renn, S., A. Götzinger; Sandoghdar, V. *Nature* **2009**, *460*, 76–80.

(7) Shields, A. J. *Nature Photonics* **2007**, *1*, 215–223.

(8) *Optical Microcavities*; Vahala, K., Ed.; World Scientific: Singapore, 2005.

(9) Mühlschlegel, P.; Eisler, H. J.; Martin, O. J. F.; Hecht, B.; Pohl, D. W. *Science* **2005**, *308*, 5728.

(10) Farahani, J. N.; Pohl, D. W.; Eisler, H. J.; Hecht, B. *Phys. Rev. Lett.* **2005**, *95*, 017402.

(11) Kühn, S.; Håkanson, U.; Rogobete, L.; Sandoghdar, V. *Phys. Rev. Lett.* **2006**, *97*, 017402.

(12) Anger, P.; Bharadwaj, P.; Novotny, L. *Phys. Rev. Lett.* **2006**, *96*, 113002.

(13) Li, J. J.; Salandrino, A.; Engheta, N. *Phys. Rev. B* **2007**, *76*, 245403.

(14) Hofmann, H. F.; Kosako, T.; Kadoya, Y. *New. J. Phys.* **2007**, *9*, 217.

(15) Taminiau, T. H.; Moerland, R. J.; Segerink, F. B.; Kuipers, L.; van Hulst, N. F. *Nano Lett.* **2007**, *7*, 28–33.

(16) Taminiau, T. H.; Stefani, F. D.; van Hulst, N. F. *Opt. Express* **2008**, *16*, 10858.

(17) Taminiau, T. H.; Stefani, F. D.; Segerink, F. B.; van Hulst, N. F. *Nature Photonics* **2008**, *2*, 234.

(18) Akimov, A. V.; Mukherjee, A.; Yu, C. L.; Chang, D. E.; Zibrov, A. S.; Hemmer, P. R.; Park, H.; Lukin, M. D. *Nature* **2007**, *450*, 402–406.

(19) Chang, D. E.; Sørensen, A. S.; Hemmer, P. R.; Lukin, M. D. *Phys. Rev. B* **2007**, *76*, 035420.

(20) Falk, A. L.; Koppens, F. H. L.; Yu, C.; Kang, K.; de Leon, N. P.; Akimov, A. V.; Jo, M.-H.; Lukin, M. D.; Park, H. *Nature Phys.* **2009**, *5*, 475–479.

(21) Balanis, C. A. *Antenna theory: Analysis and design (3rd ed.)*; Wiley-Interscience: New York, 2005.

(22) Koenderink, A. F.; Polman, A. *Phys. Rev. B* **2006**, *74*, 033402.

(23) García de Abajo, F. J.; Howie, A. *Phys. Rev. Lett.* **1998**, *80*, 5180.

(24) García de Abajo, F. J. *Phys. Rev. B* **1999**, *60*, 6086–6102.

(25) Fuller, K. A.; Kattawar, G. W. *Opt. Lett.* **1988**, *13*, 90–92.

(26) Fuller, K. A.; Kattawar, G. W. *Opt. Lett.* **1988**, *13*, 1063–1065.

(27) Sburlan, S. E.; Blanco, L. A.; Nieto-Vesperinas, M. *Phys. Rev. B* **2006**, *73*, 035403.

(28) *Handbook of optical constants of solids*; Palik, E. D., Ed.; Academic Press: New York, 1952.

(29) Novotny, L.; Hecht, B. *Principles of Nano-Optics*; Cambridge University Press: UK, 2006.

(30) Xu, Y.; Lee, R. K.; Yariv, A. *Phys. Rev. A* **2000**, *61*, 033807.

(31) Blanco, L. A.; García de Abajo, F. J. *Phys. Rev. B* **2004**, *69*, 205414.

(32) Mertens, H.; Koenderink, A. F.; Polman, A. *Phys. Rev. B* **2007**, *76*, 115123.

(33) Tai, C.-T. *Dyadic Green Functions in Electromagnetic Theory*, 2nd ed.; IEEE Press: New York, 1993.

(34) Maier, S. A.; Brongersma, M. L.; Kik, P. G.; Atwater, H. A. *Phys. Rev. B* **2002**, *65*, 193408.

(35) Koenderink, A. F.; de Waele, R.; Prangsma, J. C.; Polman, A. *Phys. Rev. B* **2007**, *76*, 201403.

(36) de Waele, R.; Koenderink, A. F.; Polman, A. *Nano Lett.* **2007**, *7*, 2004–2008.

(37) Friedler, I.; Sauvan, C.; Hugonin, J. P.; Lalanne, P.; Claudon, J.; Gérard, J.-M. *Opt. Express* **2009**, *17*, 2095–3010.

(38) Engheta, N. *Science* **2007**, *317*, 1698–1702.